

Received October 30, 2020, accepted November 17, 2020, date of publication November 24, 2020, date of current version December 10, 2020.

Digital Object Identifier 10.1109/ACCESS.2020.3040299

Receding Horizon Longitudinal Control Technology for Automatic Carrier Landing With Variable Reference Trajectory Based on Sliding Rate Information

KAIKAI CUI¹, WEI HAN¹, CONG SUN², XICHAO SU¹, AND JIE LIU^{1,3}

¹School of Basic Sciences for Aviation, Naval Aviation University, Yantai 264001, China

²Shenyang Aircraft Design and Research Institute, Shenyang 110035, China

³War Research Institute, Academy of Military Sciences, Beijing 100850, China

Corresponding author: Jie Liu (liuyexiaobao@163.com)

ABSTRACT In this paper, the longitudinal control of automatic carrier landing is studied. First, the carrier landing control problem is transformed into an optimal control problem of trajectory tracking. Considering the constraints of the control variables and the rate of change of control variables in the realistic landing process, the original linear small disturbance model is expanded. Based on the symplectic pseudospectral method and the adaptive regression prediction technology, a fast receding horizon carrier landing control technology with a variable reference trajectory is developed. Finally, the effectiveness of the control algorithm is verified by simulations at different sea states, initial deviations, and reference trajectory selection strategies. The simulation results demonstrate that the introduction of deck motion prediction can greatly reduce the phase delay of the control system and enhance the tracking ability of the carrier-based aircraft and improve the control effectiveness significantly. The proposed algorithm can precisely control the carrier landing trajectory under initial deviations, the external continuous wind disturbances, and random error of the state variables. Additionally, the calculation efficiency of the present control algorithm is sufficient for real-time online tracking.


INDEX TERMS Carrier-based aircraft, automatic carrier landing, longitudinal control, symplectic pseudospectral algorithm, receding horizon, online tracking.

I. INTRODUCTION

As the main combat weapon system of aircraft carrier formations, carrier-based aircraft greatly enhance the mastery of the seas, air superiority, and integrated attack-defense capabilities because of the high mobility. The problem of carrier landing is crucial to the effective cooperation between carrier-based aircrafts and the carrier. Carrier landing are significantly different from ground landing. Specifically, the landing area of the carrier's flight deck is limited, and the deck is constantly in motion, making the aircraft landing much more difficult. Changing meteorological conditions can cause the above adverse effects to be intensified. In order to assist the pilot in carrying out a secure carrier landing

in all weather conditions, the automatic carrier landing system (ACLS) of carrier-based manned aircraft has been greatly developed.

To ensure that the carrier-based aircraft can fly according to the ideal glide path in the ACLS system, a corresponding control algorithm must be designed to maintain the trajectory of the carrier-based aircraft. As a classical control method, Proportional Integration Differentiation (PID) control has been applied to the carrier landing control problem for many years [1], [2]. To improve the effectiveness of PID control, Zhiyuan Yang, Yimin Deng, and others have proposed a variety of parametric tuning methods utilizing intelligent optimization algorithms [3], [4]. By using these approaches, satisfactory control effectiveness has been obtained. Traditional PID control methods can achieve satisfactory landing performance in normal situations. How-

The associate editor coordinating the review of this manuscript and approving it for publication was Shihong Ding .

ever, it is difficult to track the randomly changing reference glide path under the disturbances of deck motion [5]. Hengzhi Ding used the theory of nonlinear inverse dynamics combined with PID control to design an automatic carrier landing system, which can efficiently resist carrier air wake [6]. The effectiveness of the dynamic inverse method is heavily dependent on the accuracy of the model. Therefore, the effectiveness degrades significantly when there are random wake and sea wave disturbances. To achieve better anti-interference capabilities of the ACLS, Wang *et al.* [7] developed a stable adaptive control scheme based on LDU (lower-diagonal-upper) decomposition of the high-frequency gain matrix. This approach ensures closed-loop stability and asymptotic output tracking. Zhen *et al.* [8] studied a multi-variable model reference adaptive control (MRAC) scheme for the automatic carrier-landing of unmanned aerial vehicles (UAVs) subject to nonlinear system dynamics, multivariable coupling, and parametric uncertainty. Lungu *et al.* [9] and Ju and Tsai [10] applied backstepping control to ground landing. The approach [10] addressed model parameter uncertainty in the path tracking process and it provided a reference for the glide path tracking problem of carrier landing. Wu *et al.* [11] studied robust carrier landing control by decoupling the height and velocity channels using an exact linearization method. Subsequently, robust controllers for each of the two channels were designed separately. In addition, many scholars have applied optimal control [12], [13], preview control [14], [15], sliding control [16], fuzzy control [17] and adaptive control [18], [19] technologies to the carrier landing trajectory control, and satisfactory control results are obtained.

The control algorithms discussed above play an important role in the research of automatic carrier landing control, and the control effect of PID algorithm has been verified in practice. However, the existing algorithms usually cannot deal with the control constraints explicitly, and when there are multiple control variables, there is no effective control allocation method. In addition, the above control algorithms generally divide the control system into multiple control loops to design separately, which is difficult to ensure the optimization of the whole control system.

Carrier landing control is essentially a trajectory tracking problem, so some related control techniques proposed in recent years, such as quantized static output feedback control [20], [21], non-smooth control [22], homogeneous domination approach [23] and model predictive control (MPC) [24] can also be used for reference. Among the above methods, the MPC method has the unique advantage in its ability to treat constrained problem and utilize the forecast information. These abilities are very expected for automatic carrier landing. However, the basic idea of the MPC method is to solve a finite horizon open-loop optimal control problem at each sampling instant. Hence, the solving efficiency is the bottleneck that limits its wide application in automatic carrier landing. Various numerical methods for solving nonlinear optimal control have been developed, which can be roughly

divided into direct methods and indirect methods [25]. In the last two decades, pseudospectral methods have become the most popular in the field of aeronautics and astronautics due to its high precision and sound robustness [26]. For years, pseudospectral methods were merely studied under the framework of direct methods. However, as a kind of discretization schemes, its application should not be limited only to direct methods. Recently, by utilizing the pseudospectral scheme, Peng and Wang *et al.* creatively develop a series of symplectic pseudospectral methods under the framework of indirect methods [27], [28]. These symplectic pseudospectral methods have excellent efficiency and accuracy due to the structure-preserving property [29]. And the successive convexification technique is integrated to further achieve excellent numerical robustness and fast convergence [30]. Various numerical tests demonstrate that the symplectic pseudospectral method is an appealing numerical method for solving trajectory planning problems [31], [32]. Owing to the good numerical characteristic of symplectic pseudospectral methods, together with the idea of receding horizon control, a fast receding horizon carrier landing control technology with the variable reference trajectory based on the glide rate information is designed in this paper. The contribution of this work is threefold.

First, the phase delay of the control system is greatly reduced by introducing prediction of the deck motion and the expected glide rate information into the selection progress of the reference trajectory. As a result, the following capability of the carrier-based aircraft with respect to deck motion can be significantly enhanced. Second, the derivative constraint problem of control variables in the actual control system is handled by augmenting the linear model to produce a control law that meets the requirements of practical engineering tasks. Third, by introducing Runge-Kutta integration into the original optimal tracking control method based on Receding Horizon Control (RHC), the influence of aerodynamic wake disturbances during the landing process are easily dealt with, and the simulation results are ensured to be realistic.

The remainder of this paper is structured as follows. In Section II, the problem definition and models are formulated. These models include the longitudinal linear model of small disturbances, the deck motion model, and the carrier air wake model. Section III describes the receding horizon optimal control algorithm for carrier landing based on symplectic pseudospectral algorithm. Section IV presents simulation results testing the control algorithm. Finally, Section V briefly summarizes the conclusions and discusses the further research orientation.

II. LONGITUDINAL CONTROL MODEL OF CARRIER LANDING

A. LONGITUDINAL SMALL DISTURBANCE EQUATION OF CARRIER LANDING

Compared with lateral carrier landing control, longitudinal control is more difficult and the control performance

have a greater impact on the final landing appearance. So only the longitudinal control problem is discussed in this paper.

In this paper, the linear small disturbance equations of the F/A-18A in the longitudinal direction are used to describe the landing process of the carrier-based aircraft [3], [33]:

$$\begin{cases} \dot{\mathbf{x}} = \mathbf{A}_M \mathbf{x} + \mathbf{B}_M \mathbf{u} + \mathbf{E}_M \alpha_g \\ \mathbf{x} = [\Delta v/V_0, \Delta\alpha, \Delta\theta, \Delta q, \Delta h/V_0]^T \\ \mathbf{u} = [\Delta\delta_H, \Delta\delta_{LEF}, \Delta\delta_{RT}, \Delta\delta_{PL}]^T \end{cases} \quad (1)$$

where Δv , $\Delta\alpha$, $\Delta\theta$, Δq , Δh represent the velocity, angle of attack, pitch angle, pitch angular velocity, and altitude deviation of the aircraft relative to the nominal state, respectively. $\Delta\delta_H$, $\Delta\delta_{LEF}$, $\Delta\delta_{RT}$, $\Delta\delta_{PL}$ represent the deviation of horizontal tail deflection, leading-edge flap deflection, rudder toe-in deflection, and engine throttle control angle, respectively. α_g represents the deviation in attack angle caused by vertical wind disturbances. With the exception of δ_{PL} , the above variables are all in international standard units. The unit of δ_{PL} is deg. The trim state of carrier-based aircraft is: $V_0 = 69.96m/s$, $\alpha_0 = 8.3^\circ$, $\gamma_0 = -3^\circ$. In actual flight control systems, there are some limits on the range and rate of change of the rudder deflection and throttle control angle. These limits result in the following limitations on the control variables in the carrier landing control model:

$$\begin{cases} \delta_H^{\min} - \bar{\delta}_H \leq \Delta\delta_H \leq \delta_H^{\max} - \bar{\delta}_H \\ \delta_{LEF}^{\min} - \bar{\delta}_{LEF} \leq \Delta\delta_{LEF} \leq \delta_{LEF}^{\max} - \bar{\delta}_{LEF} \\ \delta_{RT}^{\min} - \bar{\delta}_{RT} \leq \Delta\delta_{RT} \leq \delta_{RT}^{\max} - \bar{\delta}_{RT} \\ \delta_{PL}^{\min} - \bar{\delta}_{PL} \leq \Delta\delta_{PL} \leq \delta_{PL}^{\max} - \bar{\delta}_{PL} \\ |\Delta\dot{\delta}_H| \leq \dot{\delta}_H^{\max}, \quad |\Delta\dot{\delta}_{LEF}| \leq \dot{\delta}_{LEF}^{\max} \\ |\Delta\dot{\delta}_{RT}| \leq \dot{\delta}_{RT}^{\max}, \quad |\Delta\dot{\delta}_{PL}| \leq \dot{\delta}_{PL}^{\max} \end{cases} \quad (2)$$

In Eq. (2), the superscript $\bar{*}$ donates the nominal value of rudder deflection or throttle control angle, and $*^{\max}$, $*^{\min}$ represent the maximum and minimum permissible values of the variable, respectively.

B. DECK MOTION MODEL

When an aircraft carrier is at sea, it is subject to pitching, rolling, and heave motions due to both wind and waves. The pitching and heave motions of the carrier have the greatest impact on the longitudinal landing accuracy of the carrier-based aircraft. The pitching and heave motion model of the carrier deck for a carrier sailing at a typical speed of 15.4m/s can be found in Reference [34]:

$$\begin{cases} \theta_S = 0.5 \sin(0.6t + \varphi_1) + 0.3 \sin(0.63t + \varphi_1) - 0.25 \\ Z_S = 4.0 \sin(0.6t + \varphi_2) + 1.0 \sin(0.2t + \varphi_2) \end{cases} \quad (3)$$

where φ_1 and φ_2 are the random initial phases.

C. CARRIER AIR WAKE MODEL

In the present work, the engineering model of carrier air wake in Reference [34] is adopted. Since the longitudinal landing

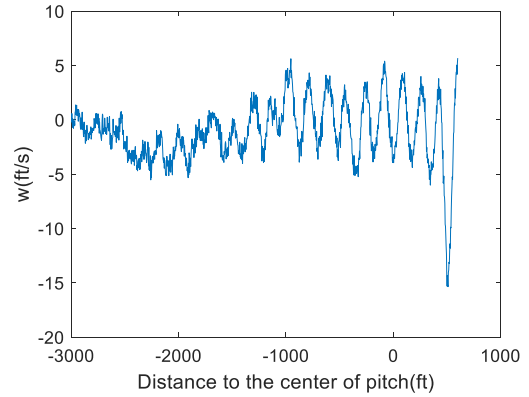


FIGURE 1. The flow field of the carrier air wake in vertical direction.

dynamics model is only affected by the air wake of vertical direction in Eq. (1), only the simulation result of air wake in vertical direction is presented in Fig. 1.

III. RECEDING HORIZON OPTIMAL CONTROL ALGORITHM FOR CARRIER LANDING

A. TRAJECTORY TRACKING OPTIMAL CONTROL PROBLEM

The optimal control problem with constraints can be written as follows:

$$\begin{cases} \min J = \int_{t_0}^{t_0+T} S(\mathbf{x}, \mathbf{u}, t) dt \\ s.t. \\ \dot{\mathbf{x}} = \mathbf{f}(\mathbf{x}, \mathbf{u}, t) \\ \mathbf{h}(\mathbf{x}, \mathbf{u}, t) \leq \mathbf{0} \end{cases} \quad (4)$$

where $S(\mathbf{x}, \mathbf{u}, t)$ is the objective function of the optimal control system. $\mathbf{f}(\mathbf{x}, \mathbf{u}, t)$ represents the dynamic model of the control system. The inequality $\mathbf{h} \leq \mathbf{0}$ refers to constraints of the actual control system, including state variable constraints and control variable constraints.

In the present paper, a symplectic pseudospectral algorithm based on the second kind of generating function [28] is used to solve the optimal control problem in the receding time window. As an indirect numerical methods for optimal control problems [35], this approach is known to have high calculation efficiency and fast convergence speed and can deal with the optimal control problem with constraints on state and control variables. Without losing generality, Eq. (4) can be rewritten as:

$$\begin{cases} \min J = \int_{t_0}^{t_0+T} \left(\mathbf{x}^T \mathbf{E} + \mathbf{u}^T \mathbf{F} + \frac{1}{2} \mathbf{x}^T \mathbf{P} \mathbf{x} + \mathbf{u}^T \mathbf{Q} \mathbf{x} + \frac{1}{2} \mathbf{u}^T \mathbf{R} \mathbf{u} \right) dt \\ s.t. \\ \dot{\mathbf{x}} = \mathbf{A} \mathbf{x} + \mathbf{B} \mathbf{u} + \mathbf{W}, \mathbf{x}(t_0) = \mathbf{x}_0 \\ \mathbf{C} \mathbf{x} + \mathbf{D} \mathbf{u} + \mathbf{V} \leq \mathbf{0} \end{cases} \quad (5)$$

where,

$$\begin{cases} E = \frac{\partial S(x, u, t)}{\partial x} \\ F = \frac{\partial S(x, u, t)}{\partial u} \\ P = \frac{\partial^2 S(x, u, t)}{\partial x^2} \\ Q = \frac{\partial^2 S(x, u, t)}{\partial u \partial x} \\ R = \frac{\partial^2 S(x, u, t)}{\partial u^2} \end{cases} \begin{cases} A = \frac{\partial f(x, u, t)}{\partial x} \\ B = \frac{\partial f(x, u, t)}{\partial u} \\ W = f - Ax - Bu \\ C = \frac{\partial h(x, u, t)}{\partial x} \\ D = \frac{\partial h(x, u, t)}{\partial u} \\ V = h - Cx - Du \end{cases} \quad (6)$$

By introducing a non-negative relaxation vector α , the inequality constraint in Eq. (5) can be rewritten as an equality constraint as follows:

$$cx + Du + v + \alpha = 0 \quad (7)$$

Furthermore, by introducing the costate vector λ and Lagrangian multiplier μ , the optimal control problem with constraints can be transformed into an unconstrained optimal control problem. As a result, the objective function can be expressed as:

$$J = \int_{t_0}^{t_0+T} (H - \lambda^T \dot{x}) dt \quad (8)$$

where H is the Hamilton function given by:

$$\begin{aligned} H(x, u, \lambda, \beta, \alpha) \\ = x^T E + u^T F + \frac{1}{2} x^T P x + u^T Q x + \frac{1}{2} u^T R u \\ + \lambda^T (Ax + Bu + W) + \mu^T (Cx + Du + V + \alpha) \end{aligned} \quad (9)$$

According to the parametric variational principle, when the objective function J achieves a minimum value, the following equations should be satisfied simultaneously:

$$\begin{cases} \frac{\partial H}{\partial u} = F + Qx + Ru + B^T \lambda + D^T \mu = 0 \\ \dot{x} = \frac{\partial H}{\partial \lambda} = Ax - BR^{-1} (F + Qx + B^T \lambda + D^T \mu) + W \\ \dot{\lambda} = -\frac{\partial H}{\partial x} = -E - Px + Q^T R^{-1} (F + Qx + B^T \lambda + D^T \mu) \\ -A^T \lambda - C^T \mu \end{cases} \quad (10)$$

According to the inequality constraints and the KKT (Karush Kuhn Tucker) condition:

$$\begin{cases} Cx - DR^{-1} (F + Qx + B^T \lambda + D^T \mu) + V + \alpha = 0 \\ \alpha^T \mu = 0, \mu \geq 0, \alpha \geq 0 \end{cases} \quad (11)$$

Eq. (5) is an optimal control problem with a Mayer type objective function and a fixed terminal time. Therefore, when

the terminal state is fixed, the boundary condition $x(t_0 + T) = x_f$ should be added. When the terminal state is free, $\lambda(t_0 + T) = 0$ must be satisfied.

The time interval $[t_0, t_0 + T]$ is divided into M sub-intervals, and each subinterval is transformed from $\Gamma_j = [t_{j-1}, t_j]$ to $[-1, 1]$ by the linear transformation $\tau = \frac{2t - t_j - t_{j-1}}{t_j - t_{j-1}}$. In the j th sub-interval, the variables x , λ , μ and α are discretized by the $N^{(j)}$ th Legendre-Gauss-Lobatto (LGL) nodes:

$$\begin{cases} x^{(j)}(\tau) = \sum_{i=0}^{N^{(j)}} x_i^{(j)} \rho_i^{(j)}(\tau), & \lambda^{(j)}(\tau) = \sum_{i=0}^{N^{(j)}} \lambda_i^{(j)} \rho_i^{(j)}(\tau) \\ \mu^{(j)}(\tau) = \sum_{i=0}^{N^{(j)}} \mu_i^{(j)} \rho_i^{(j)}(\tau), & \alpha^{(j)}(\tau) = \sum_{i=0}^{N^{(j)}} \alpha_i^{(j)} \rho_i^{(j)}(\tau) \end{cases} \quad (12)$$

where $\rho_i^{(j)}(\tau)$ is the Lagrangian interpolation polynomial corresponding to the LGL nodes in the j th sub-interval. The specific expression for this polynomial can be found in Reference [28].

Applying the stagnation point condition of the second generating function [27], [36] in the j th sub-interval, then

$$K^{(j)} \begin{bmatrix} x_{j-1} \\ \bar{x}^{(j)} \\ \bar{\lambda}^{(j)} \\ \lambda_j \end{bmatrix} + \xi^{(j)} \hat{\mu}^{(j)} + \zeta^{(j)} = r^{(j)} \quad (13)$$

According to the constraint in Eq. (7) and the complementarity condition, the following relationship can be obtained in the subinterval Γ_j

$$\begin{cases} G^{(j)} \hat{x}^{(j)} - H^{(j)} \hat{\lambda}^{(j)} - M^{(j)} \hat{\mu}^{(j)} + \hat{v}^{(j)} + \hat{\alpha}^{(j)} = 0 \\ \hat{\alpha}^{(j)} \geq 0, \hat{\mu}^{(j)} \geq 0, \hat{\mu}^{(j)} \hat{\alpha}^{(j)} = 0 \end{cases} \quad (14)$$

By assembling Eq. (13~14) in every interval according to the boundary conditions, the two-point boundary value problem in $[t_0, t_0 + T]$ can be rewritten as follows,

$$\begin{cases} a : K \begin{bmatrix} \hat{x} \\ \hat{\lambda} \end{bmatrix} + \xi \hat{\mu} + \zeta = r \\ b : G \hat{x} - H \hat{\lambda} - M \hat{\mu} + \hat{v} + \hat{\alpha} = 0 \\ c : \hat{\alpha} \geq 0, \hat{\mu} \geq 0, \hat{\mu} \hat{\alpha} = 0 \end{cases} \quad (15)$$

where, \hat{x} , $\hat{\lambda}$ and $\hat{\mu}$ contain the information of state vectors, costate vectors, and Lagrange multipliers at each of the LGL collocation points, respectively. According to Eq. (15a), the variables \hat{x} and $\hat{\lambda}$ can be expressed as linear functions of $\hat{\mu}$ separately. Therefore, the two-point boundary value problem given in Eq. (15) can be transformed into a standard linear complementarity problem based on Eq. (15b) and Eq. (15c), as shown in Eq. (16). The variable $\hat{\mu}$ can be solved using the Lemke method [37], and \hat{x} and $\hat{\lambda}$ can be solved according to the linear functions. Finally, the required

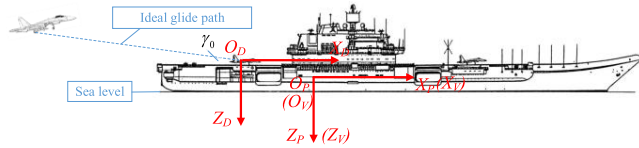


FIGURE 2. Coordinate systems of aircraft and carrier during carrier landing.

control variable u is obtained by substituting \hat{x} and $\hat{\lambda}$ into Eq. (10)

$$\begin{cases} Y\hat{\mu} + q \geq 0 \\ \hat{\mu} \geq 0 \\ \hat{\mu}^T (Y\hat{\mu} + q) = 0 \end{cases} \quad (16)$$

A detailed derivation process of the symplectic pseudospectral algorithm based on the second kind of generating function, as well as the meaning and specific expressions of the variables involved in Eq. (13)-(16), can be found in the Reference [28], [36].

B. LONGITUDINAL OPTIMAL CONTROL MODEL OF CARRIER LANDING

An aircraft must attempt to follow the ideal glide path during carrier landing process. The terminal point of the ideal glide path is located on the ideal landing point of the carrier deck. The inclination angle of the glide path is expressed as γ , as shown in Fig. 2. In Fig. 2, the coordinate systems O_D and O_P represent the deck coordinate system and the pitch coordinate system, respectively. The coordinate origin of O_D is the ideal landing point on the deck, while the coordinate origin of O_P is the pitch center of the aircraft carrier. The X -axes are both parallel to the straight section of the carrier deck and are directed forward. The Z -axes are both perpendicular to the deck and are directed vertically downward with respect to the deck. A virtual inertial coordinate system O_V is defined to represent the average motion of the aircraft carrier. O_V is primarily used to describe the base motion of the aircraft carrier. The average position of the carrier's pitch center during the navigation progress is taken as the coordinate origin, the X -axis is oriented to the average speed direction of the carrier's pitch center, and the Z -axis is perpendicular to the sea level and points downward. This coordinate system coincides with O_P when the carrier is stationary.

During landing, it is necessary to track the ideal glide path under the constraints of flight dynamics, control variables, and state variables. The tracking error must be as small as possible, and the control process must be sufficiently stable during the trajectory tracking process. Based on the above analysis, the mathematical model of the optimal landing control problem of carrier-based aircraft can be described as

Eq. (17),

$$\begin{cases} \min J = \frac{1}{2} \int_{t_0}^{t_0+T} [(X - X_e)^T \bar{P}(X - X_e) + U^T \bar{R}U] dt \\ s.t. \\ \dot{X} = \bar{A}X + \bar{B}U + \bar{E}\alpha_g \\ X^{\min} \leq X \leq X^{\max}, \quad U^{\min} \leq U \leq U^{\max} \end{cases} \quad (17)$$

where X_e represents the ideal flight path of the carrier-based aircraft and X represents the actual flight path of the carrier-based aircraft, which can be regarded as the actual state variable of the system here. U represents the actual control input. \bar{P} and \bar{R} are the diagonal coefficient matrices. \bar{P} is required to be semi-positive definite while \bar{R} must be positive definite. The symbol \leq indicates that each component of the two vectors must satisfy an \leq inequality. It can be seen from Eq. (5) that the rate of change of control inputs cannot be limited in Eq. (5), while the limit conditions on rates of change exist in Eq. (2). So the original dynamic model given in Eq. (1) is extended by setting $X = [x^T : u^T]^T$ and $U = \dot{u}$, which makes Eq. (5) applicable for practical engineering problems. Accordingly, the relationship between \bar{A} , \bar{B} , \bar{E} and A_M , B_M , E_M can be obtained as:

$$\begin{cases} \bar{A} = \begin{bmatrix} A_M & B_M \\ \dots & \dots \\ \mathbf{0}_{4 \times 9} \end{bmatrix} & \bar{B} = \begin{bmatrix} \mathbf{0}_{5 \times 4} \\ \dots \\ I_4 \end{bmatrix} & \bar{E} = \begin{bmatrix} E_M \\ \dots \\ \mathbf{0}_{4 \times 1} \end{bmatrix} \end{cases} \quad (18)$$

According to Eq. (6), (17) and (2), it can be shown that:

$$\begin{cases} A = \bar{A} \\ B = \bar{B} \\ W = \mathbf{0} \\ E = \bar{P}(X - X_e) \end{cases} \quad \begin{cases} F = \bar{R}U \\ P = \bar{P} \\ Q = \mathbf{0} \\ R = \bar{R} \end{cases} \quad (19)$$

$$\begin{cases} C = \begin{bmatrix} \mathbf{0}_{4 \times 5} & I_4 \\ \mathbf{0}_{4 \times 5} & -I_4 \\ \mathbf{0}_{8 \times 9} \end{bmatrix}, & D = [\mathbf{0}_{4 \times 8} I_4 - I_4]^T \\ V = \left[-\left(X_{(6:9)}^{\max}\right)^T \left(X_{(6:9)}^{\min}\right)^T - \left(U^{\max}\right)^T \left(U^{\min}\right)^T \right]^T \end{cases} \quad (20)$$

where the subscript ($a: b$) represents the a -th to the b -th components of the vector. It should be pointed out that the expression of W obtained from Eq. (6) is $W = \bar{E}\alpha_g$. In Eq. (19), the physical quantity α_g is caused by random wind disturbances. Additionally, the information of wind disturbance in the time interval $[t_0, t_0 + T]$ cannot be obtained or predicted at t_0 . Therefore, the random disturbance cannot be handled when solving the optimal control model. To address this, this component of interference can be ignored in the model solving process, i.e. $W = \mathbf{0}$. The error caused by this simplification will be discussed in Section III-C.

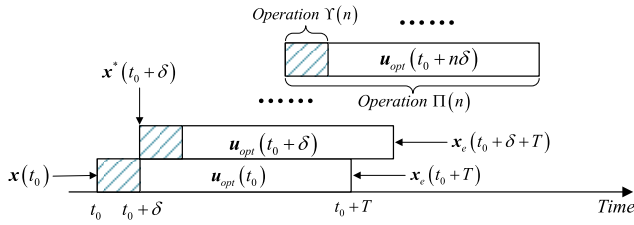


FIGURE 3. Time series diagram of VTGR-RHC algorithm.

C. RHC ALGORITHM FOR CARRIER LANDING WITH VARIABLE REFERENCE TRAJECTORY BASED ON GLIDE RATE INFORMATION (VTGR-RHC)

1) VTGR-RHC ALGORITHM

Inspired by Reference [38], a receding horizon carrier landing control algorithm with variable reference trajectory is designed in the present paper. The core idea of the receding horizon control method is to solve the optimal control problem over a specified future time interval and treat the resulting optimal control law at the current time as the actual input of the control system until the next calculation time point to repeat the process [39]. A time-series diagram of the VTGR-RHC algorithm is given in Fig. 3.

The symbols used in Fig. 3 are explained as follows:

$x_e(t)$: The desired state of the control system at time t .

$x^*(t)$: The actual state of the control system at time t .

Operation $\Pi(n)$: Over the time interval $\Lambda_n = [t_0 + n\delta, t_0 + n\delta + T]$, according to the two-point boundary condition $x(t_0 + n\delta) = x^*(t_0 + n\delta)$, $x(t_0 + n\delta + T) = x_e(t_0 + n\delta + T)$ and the expected glide path $x_e^n(t)$, Eq. (17) is solved using the symplectic pseudospectral algorithm introduced in Section III-A, where the matrices are selected according to Eq. (19)-(20).

$u_{opt}(t_0 + n\delta)$: The optimal control law obtained by the calculation of *Operation* $\Pi(n)$ over the time period $[t_0 + n\delta, t_0 + n\delta + T]$.

Taking $u_{opt}(t_0 + n\delta)$, $x^*(t_0 + n\delta)$ as the actual control input of the system and the initial condition, respectively, $x^*(t_0 + (n+1)\delta)$ is obtained by integrating the real control system of Eq. (17) in $[t_0 + n\delta, t_0 + (n+1)\delta]$. The numerical integration method used in the present work is the Fourth-order-Runge-Kutta algorithm. By introducing the aerodynamic wake influence into the simulation process, the simulation error caused by the simplification of the matrix W in Eq. (19) can be eliminated.

2) SELECTION OF THE REFERENCE GLIDE PATH

According to the carrier landing optimal control model given in Eq. (17), there is a standard reference trajectory to be tracked in the process of carrier landing. However, when the aircraft carrier is at sea, it is accompanied by six degrees of freedom motion due to the wind and waves. As a result, the ideal landing point will move in response to the carrier deck motion. If the deck motion is ignored, the initial ideal landing trajectory will always be tracked as the straight

trajectory. This can lead to significant landing errors. In order to solve this problem, two strategies can be adopted:

a. The real-time motion information of the aircraft carrier can be monitored, and the straight-line trajectory between the current position of the carrier-based aircraft and the ideal landing point is regarded as the reference trajectory in the current time window.

b. The motion of the carrier can be predicted, and the future position of the ideal landing point is predicted. Subsequently, the straight-line trajectory between the current position of the carrier-based aircraft and the predicted position of the ideal landing point is used as the reference trajectory in the current time window.

The two strategies above correspond to two different ideal glide paths, as shown in Fig. 4. The hexagon stars in the figure represent the different positions of the ideal landing point according to the different strategies. Compared to Strategy (b), Strategy (a) is relatively simple and does not require a prediction of the deck motion. However, it can be seen from the later simulation results that the reference glide path generated by Strategy (a) results in a significant phase delay and poor control. Therefore, the present work is focused on Strategy (b).

3) PREDICTION OF AIRCRAFT CARRIER DECK MOTION

According to Strategy (b), an ideal glide slope based on predicted deck motion needs to be generated. In order to improve the efficiency of the algorithm, an autoregressive (AR) prediction algorithm is selected to predict the deck motion. The AR prediction model of p -th order can be simplified as [40]:

$$\xi_t = a_1\xi_{t-1} + a_2\xi_{t-2} + \dots + a_p\xi_{t-p} + \zeta_t \quad (21)$$

where ξ is the variable to be predicted, ξ_{t-j} , $j = 0, 1, 2 \dots p$ represent the historical data of ξ , a_j , $j = 1, 2 \dots p$ are undecided variables, and ζ_t donates random white noise. Define $\xi_N = [\xi_{p+1}, \xi_{p+2}, \dots, \xi_N]^T$ and $\mathbf{a}_N = [a_1, a_2, \dots, a_p]^T$, and

$$\mathbf{A}_N = \begin{bmatrix} \xi_p & \xi_{p-1} & \dots & \xi_1 \\ \xi_{p+1} & \xi_p & \dots & \xi_2 \\ \dots & \dots & \dots & \dots \\ \xi_{N-1} & \xi_{N-2} & \dots & \xi_{N-p} \end{bmatrix} \quad (22)$$

where N donates the number of historical data used for forecasting. In order to minimize the objective function $Cost = (\xi_N - \mathbf{A}_N \mathbf{a}_N)^T (\xi_N - \mathbf{A}_N \mathbf{a}_N)$, the least-squares method is used to estimate the undetermined coefficients, and the optimal estimated value of \mathbf{a}_N is obtained as

$$\hat{\mathbf{a}}_N = (\mathbf{A}_N^T \mathbf{A}_N)^{-1} \mathbf{A}_N^T \xi_N \quad (23)$$

To ensure that Eq. (23) is meaningful, when \mathbf{A}_N is not column full rank, the singular value decomposition $\mathbf{A}_N = \mathbf{U} \mathbf{\Sigma} \mathbf{V}^T$ can be applied and $(\mathbf{A}_N^T \mathbf{A}_N)^{-1} \mathbf{A}_N^T$ in Eq. (23) can be replaced by $\mathbf{V} \mathbf{\Sigma}^{-1} \mathbf{U}^T$. Then the data at the next l steps can be predicted by the following equation:

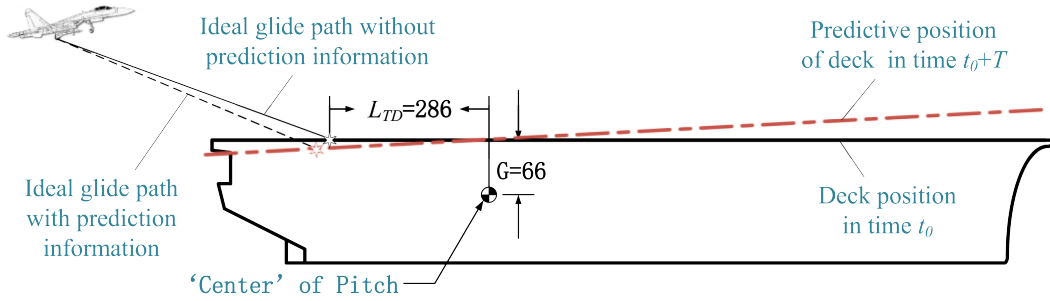


FIGURE 4. Comparison of reference trajectory selection strategies.

$$\hat{\xi}_{N+l} = \begin{cases} \sum_{j=1}^p \hat{a}_j \hat{\xi}_{N+l-j} & l = 1 \\ \sum_{j=1}^l \hat{a}_j \hat{\xi}_{N+l-j} + \sum_{j=l+1}^p \hat{a}_j \hat{\xi}_{N+l-j} & 1 < l \leq p \\ \sum_{j=1}^p \hat{a}_j \hat{\xi}_{N+l-j} & l > p \end{cases} \quad (24)$$

When the AR algorithm is applied to predict the deck motion, the prediction step length t_p , the maximum prediction step l_m , the model order p and the number of historical data N should be determined first. Generally, t_p and l_m can be determined according to the problem. Numerical simulation experiments based on the actual problem can be carried out to determine p and N . The order of the model p can be also determined by the AIC criterion or SBC criterion [41].

4) DESIGN OF THE REFERENCE TRAJECTORY BASED ON GLIDE RATE INFORMATION

After the predicted aircraft carrier motion is obtained, the corresponding glide rate of the reference trajectory in time interval $[t_0 + n\delta, t_0 + n\delta + T]$ can be calculated. It can be seen from Fig.4 that, without considering the aircraft carrier motion, the ideal landing point in O_P is $P_D = [-L_{TD}, -G]$. The actual position of the carrier-based aircraft in O_V is $P_F = [X_{FR}, Z_{FR}]$ and the position of the stern in O_V is $P_t = [X_t^v, Z_t^v]$. The position vector of the ideal landing point relative to its original position in O_V can be expressed as

$$R_D^v = \begin{bmatrix} X_D^v \\ Z_D^v \end{bmatrix} = P_D^v - P_D \quad (25)$$

where, P_D^v is the position vector of the ideal landing point in O_V , Further, the expected glide rate of the carrier-based aircraft can be calculated as

$$K_{gp} = \kappa \frac{Z_D^v - \Delta h}{t_r} \quad (26)$$

where t_r is the expected remaining time for carrier-based aircraft to reach the touchdown point. Δh represents the height error between the aircraft and the virtual ideal landing point, $\kappa = \zeta \cdot (X_D^v - L_{TD} - X_{FR})$ is the regulatory factor. The reason for the introduction of κ is that when the carrier-based aircraft approaches the ideal landing point, the value of K_{gp} becomes

rather large due to the small value of t_r . This can exceed the control ability of the actuator and result in a divergence of the calculation. The introduction of κ also increases the following capability of the carrier-based aircraft at the beginning of the landing phase. For t_r can be calculated as:

$$t_r = \frac{X_D^v - L_{TD} - X_{FR}}{V_0 \cdot \cos \gamma_0 - V_S} \quad (27)$$

K_{gp} can be rewrote as:

$$K_{gp} = \zeta \cdot (Z_D^v - \Delta h) \cdot (V_0 \cdot \cos \gamma_0 - V_S) \quad (28)$$

The expected glide path is generated according to the expected glide rate information:

$$\Delta h_e(\Delta t) = (\Delta h + K_{gp} \Delta t) / V_0 \quad (29)$$

where, $\Delta t = t - t_0 - n\delta$. Letting $\Delta t = T$ in Eq. (29), the terminal boundary condition can be obtained as $\Delta h_e(T)$.

The receding calculation ends when the carrier-based aircraft reaches the deck,

$$\begin{cases} X_{FR} > X_t^v \\ Z_{FR} > Z_D^v - G + (X_D^v - L_{TD} - X_{FR}) \tan \theta_S \end{cases} \quad (30)$$

5) THE FRAMEWORK OF THE VTGR-RHC ALGORITHM

As described above, the VTGR-RHC algorithm is graphically summarized in Fig. 5. In order to obtain accurate longitudinal landing error, the dichotomy method is applied after RHC calculation.

IV. SIMULATION VERIFICATION

A. SIMULATION CONDITIONS

The values of matrix A_M , B_M and E_M in Eq. (1) are taken as [33]:

$$A_M = \begin{bmatrix} -0.0705 & 0.0475 & -0.1403 & 0 & -5.8 \times 10^{-5} \\ -0.3110 & -0.3430 & 0 & 0.9913 & 1.02 \times 10^{-3} \\ 0 & 0 & 0 & 1 & 0 \\ 0.0218 & -1.1660 & 0 & -0.2544 & 0 \\ 0 & -1 & 1 & 0 & 0 \end{bmatrix}$$

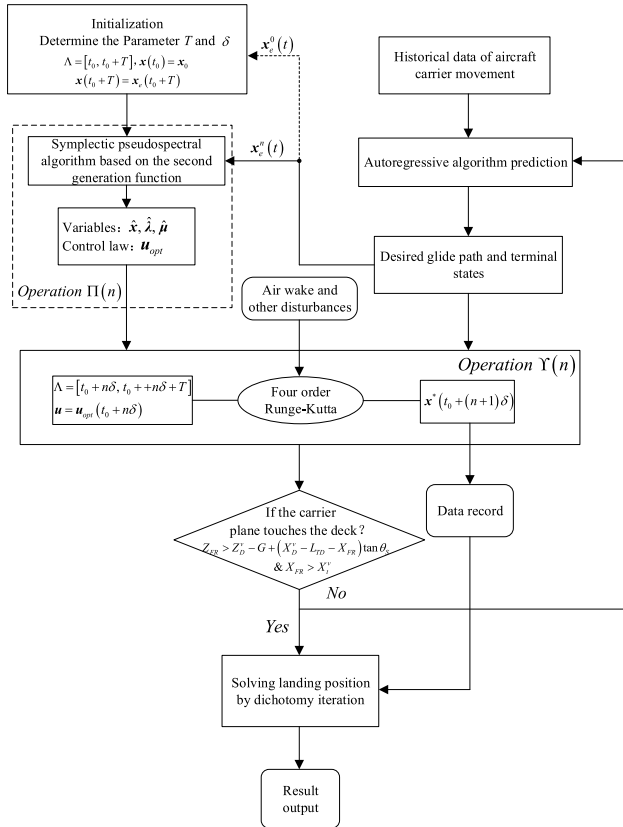


FIGURE 5. The framework of the VTGR-RHC algorithm.

TABLE 1. The constraints of the carrier-based aircraft control system.

Control variables	Range of values	Trim values	Maximum rate of change
δ_H	[-24 deg, 10.5 deg]	-11.86 deg	40 deg/s
δ_{LEF}	[-3 deg, 33 deg]	17.6 deg	15 deg/s
δ_{RT}	[-30 deg, 30 deg]	0 deg	56 deg/s
δ_{PL}	[0, 1]	0.254	0.55 deg/s

$$B_M = \begin{bmatrix} 0.0121 & 0.00248 & 0.1690 & 0.2316 \\ -0.0721 & 0.0140 & 0.0128 & -0.0338 \\ 0 & 0 & 0 & 0 \\ -1.8150 & -0.0790 & 0.1681 & 0.0023 \\ 0 & 0 & 0 & 0 \end{bmatrix}$$

$$E_M = [0.0475 \quad -0.343 \quad 0 \quad -1.166 \quad 0]^T$$

The constraints of the carrier-based aircraft control system are shown in Table 1 [12], [42].

B. THE CARRIER LANDING CONTROL EFFECTIVENESS UNDER TYPICAL SEA STATE

Under typical sea conditions, the deck motion of an aircraft carrier can be described by the model given in Section II-B. Based on the deck motion model and the simulation conditions in Section IV-A, the process of the carrier landing

control is simulated. The receding time window length is taken as 1.5s, and the receding step length is taken as 0.05s. In addition, the aircraft carrier is assumed to travel along a straight line at a fixed speed $V_S = 15.4m/s$. In order to simulate a realistic situation, a random error within $\pm 1\%$ is introduced into the state variables to replicate uncertain interference in the simulation process. The parameter ζ is taken as 0.012 based on experimental test. In order to avoid the control signal given by the algorithm exceeding the control ability of the actual actuator, the absolute value of K_{gp} in the simulation is limited to 1.5.

The control effectiveness is demonstrated in Fig. 6, where Fig. 6(a) shows the glide path of the carrier-based aircraft and Fig. 6(b) shows the variation in the height of the carrier-based aircraft during the landing process. It can be seen from Fig. 6 that by applying the VTGR-RHC algorithm the aircraft can overcome the initial error interference within 3 seconds, and then the aircraft can accurately track the deck motion and follow the ideal landing trajectory. The error between practical flight path and expected flight path is the same with the error between variation height of the plane and variation height of the ideal touch point numerically. And this error result can be found in Fig. 9 as the ‘typical sea state’, from which we can see that the altitude position error of the aircraft can be limited in 0.25 m during the steady-state control process. And the final longitudinal error of the landing point on the deck is 1.1147m.

The simulations were performed in MATLAB R2016b on an Intel Core i5-6200U personal computer with a 2.3 GHz processor and 8 GB of RAM. The single-step solution time of the algorithm was 18.7ms which was much shorter than the step length. It means the algorithm has high computational efficiency and can meet the requirements of real-time online tracking.

The rate of change of each control variable during landing is shown in Fig. 7. Fig. 7(a-d) show the rate of change of elevator deflection, leading-edge flap deflection, rudder toe-in deflection, and engine throttle control angle, respectively. It can be seen from Fig. 7 that the rate of change of elevator deflection, leading-edge flap deflection, and throttle control angle reach the performance limits of the actuators in the control process (as shown in the dotted line). This demonstrates that the algorithm can effectively limit the control variables.

The result of state variable θ is shown in Fig. 8. From Fig. 8, we can see that during the carrier landing process, the pitch angle of the aircraft only change in a small scale (about 0.7 deg in the last 10 seconds). That means the aircraft can hold a satisfied attitude for hooking cable during the carrier landing process.

C. SIMULATION RESULTS UNDER DIFFERENT SEA STATES

In this section, the effectiveness of the VTGR-RHC algorithm for carrier landing is analyzed under different sea states. The control effectiveness under typical (normal) sea state was shown in Fig. 6. The landing error results under low, medium-high and high sea states (corresponding to 0.7, 1.3,

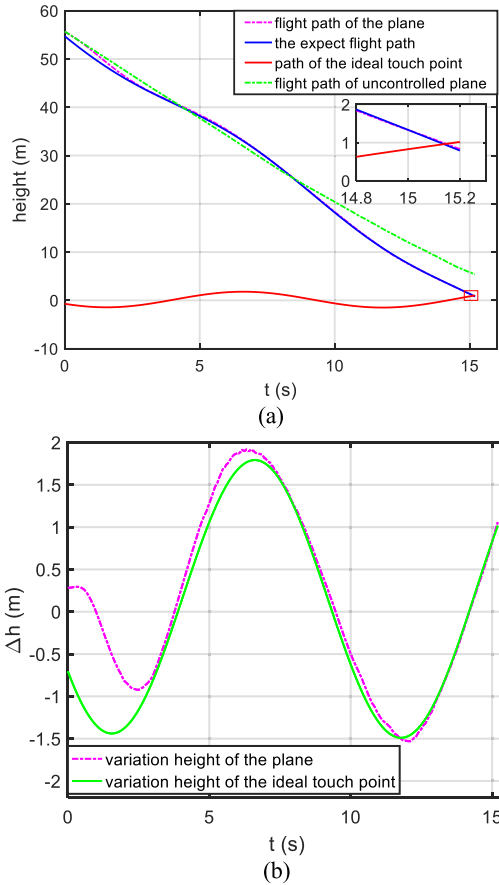


FIGURE 6. The control effect of VTGR-RCH algorithm.

and 1.6 times of deck motion and air wake intensity) are shown in Fig. 9. From Fig. 9, it can be seen that the tracking error between the carrier-based aircraft and the ideal glide path is strongly dependent on the severity of sea states.

In order to make a statistical comparison of the landing control under different sea states, 50 different initial phases of waves were selected for simulation. The longitudinal deviation of the landing position and calculation time were then calculated for each initial state. The 50 individual cases with different initial phases were simulated under each sea state, and the statistical average results are shown in Table 2. Here, to improve the performance of the control method under the complex sea states and initial phases, the parameter ζ is taken as 0.013. From the data given in Table 2, it can be seen that the landing error increases with increased severity of the sea states.

Table 2 provides the average statistics of the landing error results. In order to further analyze the distribution of landing errors, Fig. 10 shows the distribution of the 50 landing points on the deck under each sea state. It can be seen from Fig. 10 that with the increase of the sea state severity, the errors in landing accuracy as well as the error dispersion range increase gradually. Under low and normal sea states, all landing points are located between the second and the third arresting cables, which ensures the ideal situation of the third cable hooking.

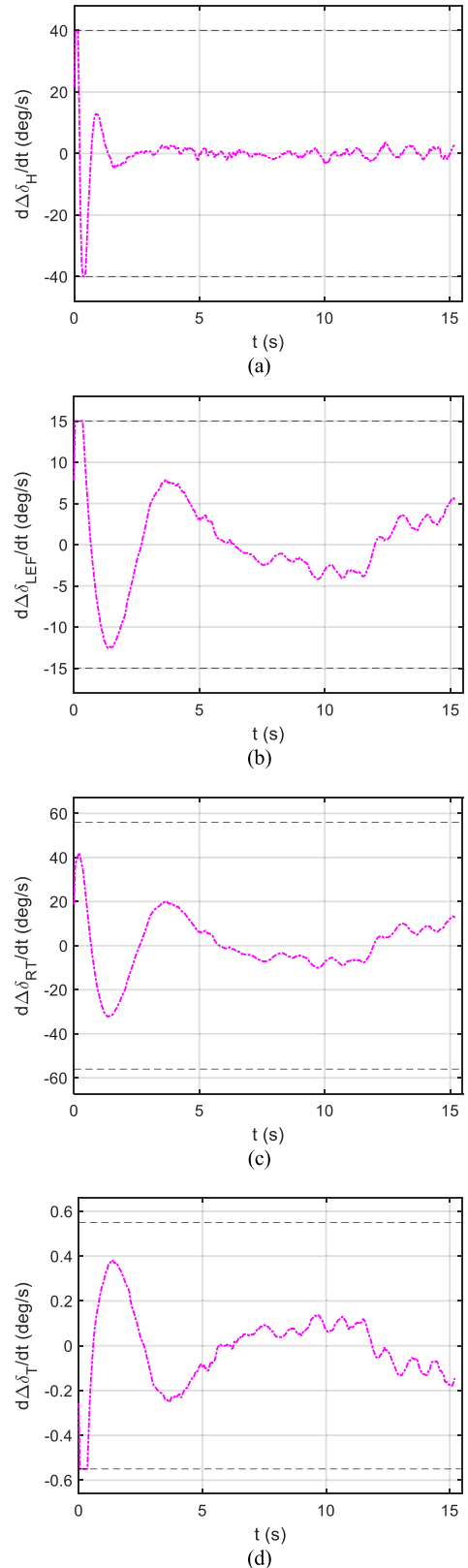


FIGURE 7. Rates of change of control variables during the landing process.

In most cases of the medium-high sea states, the carrier-based aircraft can achieve the third cable hooking, and the second cable hooking may occur on rare occasions. While under the

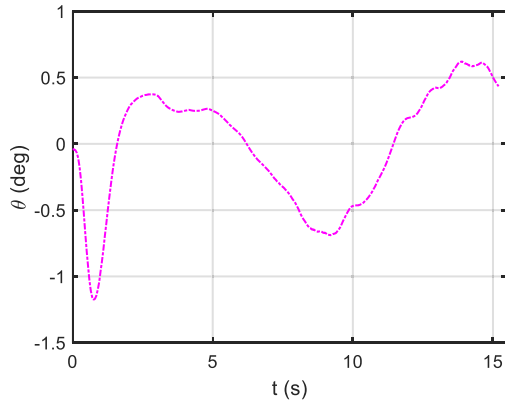


FIGURE 8. Resulting state variables during the carrier landing process.

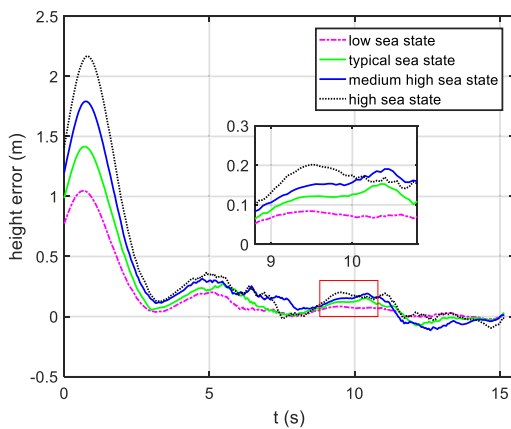


FIGURE 9. Control effect and comparison diagram under different sea states.

TABLE 2. Statistics of landing error and computation time under different sea states.

Sea state	Low sea state	Normal sea state	Medium-high sea state	High sea state
Longitudinal deviation (m)	0.8528	1.4351	2.1438	2.6397
Computation time (s)	5.3494	5.2906	5.4172	5.3181

high sea state, the fourth cable hooking may occur in some cases, which is barely acceptable in typical scenarios. These results indicate that a further increase in the severity of the sea state may lead to a landing failure. For this reason, the navies of all countries have strict rules on the sea state of carrier landing.

D. THE CARRIER LANDING CONTROL EFFECTIVENESS UNDER DIFFERENT INITIAL DEVIATION CONDITIONS

Similarly, considering the control performance of the algorithm under different initial deviation conditions, three groups of different initial errors (1.5, 0.5 and -1 times of x_0 , respectively) were selected for simulation under a typical sea state.

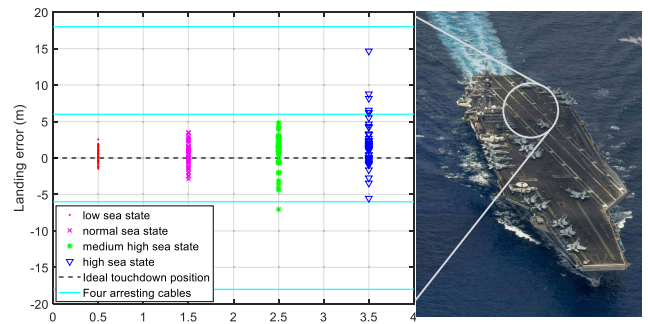


FIGURE 10. Distribution of landing points under different sea states.

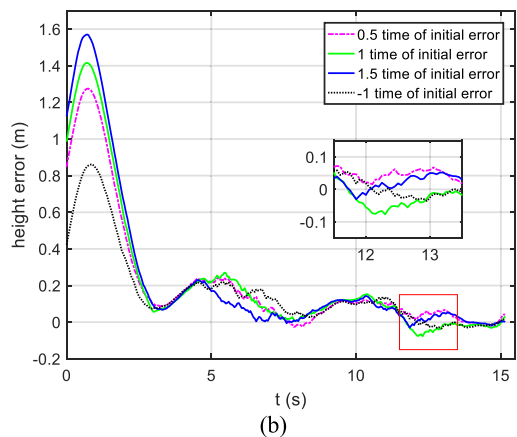
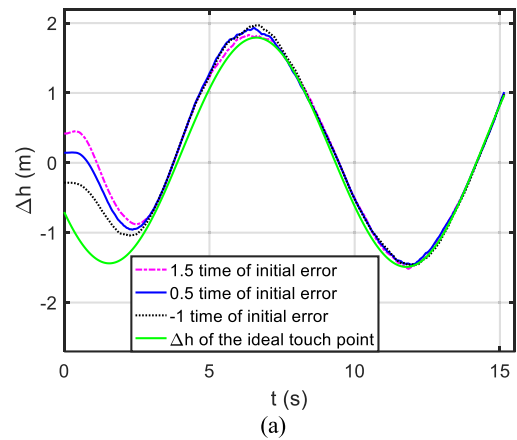


FIGURE 11. Control effectiveness and comparison under different initial deviation conditions.

The resulting control effectiveness are shown in Fig. 11(a). Fig. 11(b) shows a comparison of landing error under four different initial deviation conditions. From Fig. 11, it can be seen that the altitude control errors in the last 10 seconds under different initial error conditions are all less than 0.2m and the different initial error conditions has little influence on the final landing control effect.

A total of 50 carrier landing simulations were carried out under each initial error condition in order to produce statistics of longitudinal landing deviation and calculation time. The statistical average results are shown in Table 3. From these results, it can be seen that the average longitudinal landing

TABLE 3. Statistics of landing deviation and computation time under different initial deviation conditions.

Initial Conditions	1.5 times initial error	1 times initial error	0.5 times initial error	-1 times initial error
Longitudinal deviation(m)	1.1475	1.2551	0.9179	1.0786
Computation time (s)	5.4800	5.3359	5.4950	5.6900

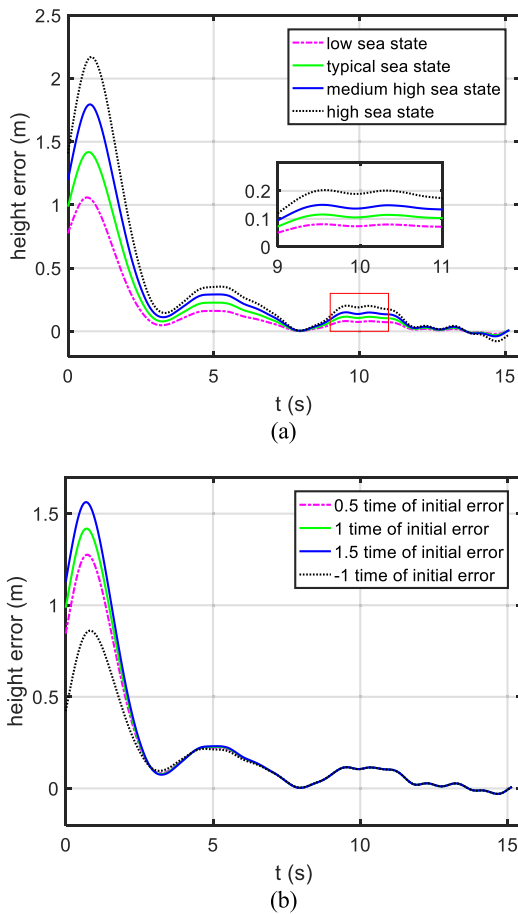


FIGURE 12. Control effectiveness comparison under different sea states and initial deviation conditions.

deviations under different initial conditions are all less than 1.3m and there is no obvious correlation between the relative size of the initial error and the final landing error. What's more, the average computation times of the whole landing process are around 5.5s, which is only about 1/3 of the real time range.

In order to further explore the influence of different sea states and different initial deviations on the final landing control effect, the two cases described above were simulated again with the error caused by random interference being ignored. The results are shown in Fig. 12. Fig.12 further

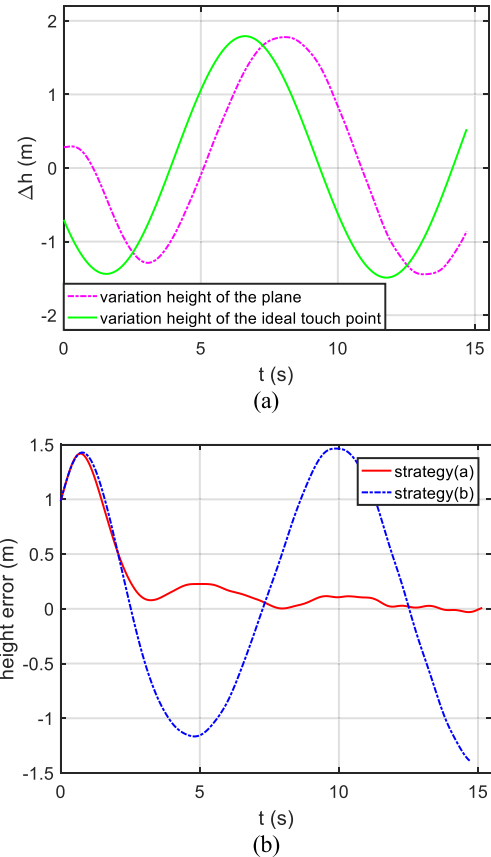


FIGURE 13. Control effect comparison of different reference trajectory selection strategies.

confirms that the tracking error between the aircraft and the ideal glide path is positively correlated to the severity of sea states. Conversely, the relative size of the initial error has no significant impact on the final landing control error.

E. CONTROL EFFECTS OF DIFFERENT REFERENCE TRAJECTORY SELECTION STRATEGIES AND CONTROL METHODS

As mentioned before, there are two strategies for the selection of the reference trajectory used in the control algorithm (described in Section III-C). Fig. 13(a) shows the control effects of Strategy (a) and Fig. 13(b) shows the control effect comparison of these two selection strategies. Compare to Fig. 6, it can be seen that the phase delay of the control system is greatly reduced by introducing prediction of the carrier deck motion in the control process. As a result, the following capability of the carrier-based aircraft to the deck motion can be enhanced. As well, the height error of the aircraft can be reduced from $\pm 1.5m$ to $\pm 0.25m$.

In the online optimal tracking control method based on RHC proposed in the literature [38], interpolation is used to obtain the state variables at the current time. This operation makes it impossible to deal with the influence of the aerodynamic wake disturbances on the carrier-based aircraft, and therefore, the simulation results do not accurately reflect

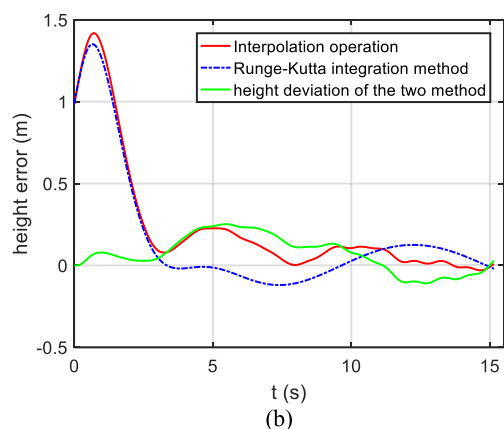
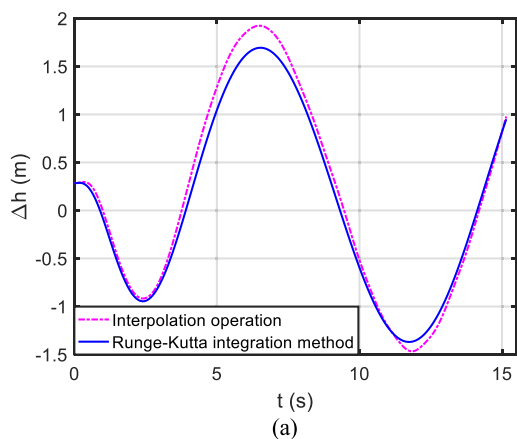


FIGURE 14. Simulation results under different state variable solving methods.

the real physical scenario. The Runge-Kutta integration technique applied in this paper can easily deal with the influence of the aerodynamic wake disturbances.

Accounting for aerodynamic wake disturbances, the two methods above were used to simulate the carrier landing control process, respectively. The results are shown in Fig. 14(a), and the height deviation of the two methods is shown in Fig. 14(b). From Fig. 14, it can be seen that the interpolation operation will lead to extra height error by a maximum of 0.25m during the simulation due to the absence of aerodynamic wake disturbance. It should be noted that the random disturbance factors were not considered in Fig.13 and Fig. 14 in order to obtain a clearer conclusion.

Finally, to confirm the algorithm’s effectiveness, comparison experiments are done using typical LQ (Linear Quadric) feedback optimal control algorithm and VTGR-RCH algorithm. The simulation result of LQ optimal control is shown in Fig. 15(a), and the height deviations of the two methods are shown in Fig. 15(b). From Fig. 15, it can be seen that the typical LQ algorithm cannot effectively track the movement of the carrier, and the steady-state error is far greater than VTGR-RCH algorithm. Within the first 2.5 seconds of the control process, the height error of typical LQ algorithm is less than that of VTGR-RCH. This is due to that the control variables cannot be constrained effectively by typical LQ

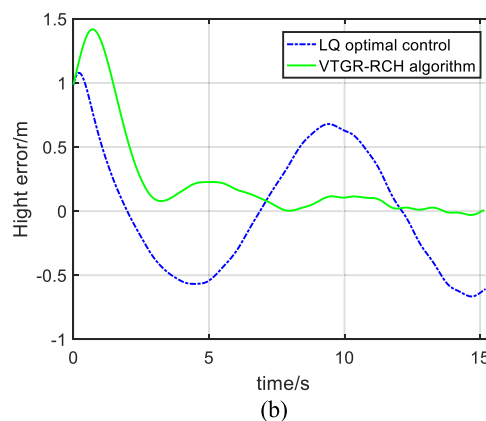
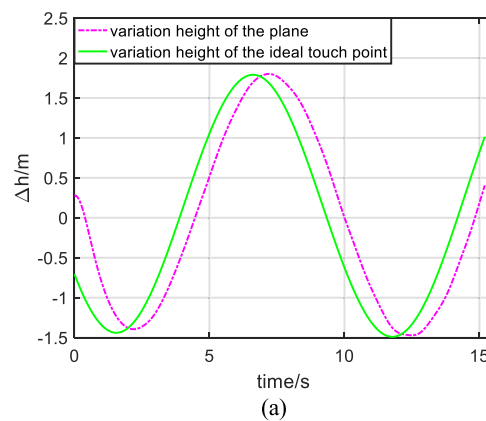


FIGURE 15. Simulation results under different state variable solving methods.

algorithm and the initial height error can be restrained rapidly under the over-limit control variables. While the over-limit control variables cannot be obtained in the real physical scenario. This also illustrates that the VTGR-RCH algorithm is more practical in the actual situation of engineering. It should be noted that the random disturbance factors were not considered in this simulation, either.

V. CONCLUSION

In this paper, the problem of longitudinal automatic carrier landing control is studied. First, the carrier landing control problem of aircraft was transformed into an optimal control problem of trajectory tracking. Further, the original linear small disturbance model was extended to account for constraints on control variables and derivatives of control variables in the landing process. With the help of a symplectic pseudospectral algorithm based on the second kind of generating function and adaptive regression prediction technology, a receding horizon carrier landing control scheme with a variable reference trajectory based on the information of the glide rate is designed. Finally, simulations were performed to demonstrate the control effectiveness of the algorithm under different sea states, initial deviations, and reference trajectory selection strategies.

The simulation results show that the proposed algorithm has the following advantages:

(1) The phase delay of the control system is greatly reduced by introducing prediction of deck motion into the reference trajectory selection. This also enhances the following ability of the aircraft and improves the landing accuracy significantly.

(2) Through the augmentation of the linear small disturbance model, the constraint problem of the control variable derivations in the control system is solved. This allows the control law generated by the algorithm to satisfy actual engineering requirements in real scenarios.

(3) The algorithm proposed in this paper can effectively control the landing trajectory of carrier-based aircraft with high accuracy in the case of initial deviation, external continuous wind disturbances, and random errors of state variables.

(4) The present algorithm has better performance comparing with the typical LQ algorithm, and the computational efficiency meets the requirements of real-time online tracking.

In this paper, the selection of the coefficient matrix, time window length, and receding step length were all obtained by experiments. Further, an intelligent optimization algorithm may be applied to further optimize these parameters so as to obtain better control effectiveness. And aiming at the carrier landing control problem with mismatched model term, some robust control methods [43], [44] can also serve as reference and guidance.

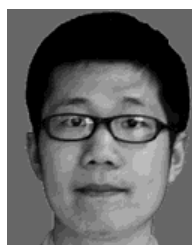
REFERENCES

- [1] D. J. Mook, D. A. Swanson, M. J. Roemer, and R. Noury, "Improved noise rejection in automatic carrier landing systems," *J. Guid., Control, Dyn.*, vol. 15, no. 2, pp. 509–519, Mar. 1992.
- [2] J. M. Urnes and R. K. Hess, "Development of the F/A-18A automatic carrier landing system," *J. Guid., Control, Dyn.*, vol. 8, no. 3, pp. 289–295, May 1985.
- [3] Z. Yang, H. Duan, Y. Fan, and Y. Deng, "Automatic carrier landing system multilayer parameter design based on cauchy mutation pigeon-inspired optimization," *Aerosp. Sci. Technol.*, vol. 79, pp. 518–530, Aug. 2018.
- [4] Y. Deng and H. Duan, "Control parameter design for automatic carrier landing system via pigeon-inspired optimization," *Nonlinear Dyn.*, vol. 85, no. 1, pp. 97–106, Mar. 2016.
- [5] Z. Zhen, S. Jiang, and K. Ma, "Automatic carrier landing control for unmanned aerial vehicles based on preview control and particle filtering," *Aerosp. Sci. Technol.*, vol. 81, pp. 99–107, Oct. 2018.
- [6] H. Ding, "Design of automatic carrier landing system based on dynamic inverse and PID control," in *Proc. 4th Int. Conf. Mechatronics, Mater., Chem. Comput. Eng.*, Xi'an, China, 2015, pp. 2330–2336.
- [7] X. Wang, X. Chen, and L. Wen, "Adaptive disturbance rejection control for automatic carrier landing system," *Math. Problems Eng.*, vol. 2016, Jul. 2016, Art. no. 7345056.
- [8] Z. Zhen, G. Tao, C. Yu, and Y. Xue, "A multivariable adaptive control scheme for automatic carrier landing of UAV," *Aerosp. Sci. Technol.*, vol. 92, pp. 714–721, Sep. 2019.
- [9] M. Lungu, "Backstepping and dynamic inversion combined controller for auto-landing of fixed wing UAVs," *Aerosp. Sci. Technol.*, vol. 96, Jan. 2020, Art. no. 105526.
- [10] H.-S. Ju and C.-C. Tsai, "Glidepath command generation and tracking for longitudinal autoland," *IFAC Proc. Volumes*, vol. 41, no. 2, pp. 1093–1098, 2008.
- [11] W. Wu, J. Wang, J. Liu, Y. Zhang, and G. An, "Carrier Landing Robust Control Based on Longitudinal Decoupling," *Trans. Nanjing Univ. Aeronaut. Astronaut.*, vol. 34, no. 6, pp. 609–616, Dec. 2017.
- [12] Y. Fan, F. H. Lutze, and E. M. Cliff, "Time-optimal lateral maneuvers of an aircraft," *J. Guid., Control, Dyn.*, vol. 18, no. 5, pp. 1106–1112, Sep. 1995.
- [13] M. Li, Z. Zhen, H. Gong, M. Hou, and S. Huang, "Optimal preview control for automatic carrier landing system of carrier-based aircraft with air wake," *Trans. Nanjing Univ. Aeronaut. Astronaut.*, vol. 34, no. 6, pp. 659–668, Dec. 2017.
- [14] S. Koo, S. Kim, and J. Suk, "Model predictive control for UAV automatic landing on moving carrier deck with heave motion," *IFAC-PapersOnLine*, vol. 48, no. 5, pp. 059–064, 2015.
- [15] Z. Zhen, S. Jiang, and J. Jiang, "Preview control and particle filtering for automatic carrier landing," *IEEE Trans. Aerosp. Electron. Syst.*, vol. 54, no. 6, pp. 2662–2674, Dec. 2018.
- [16] Y. Huang, M. Zhu, Z. Zheng, and M. Feroskhan, "Fixed-time autonomous shipboard landing control of a helicopter with external disturbances," *Aerosp. Sci. Technol.*, vol. 84, pp. 18–30, Jan. 2019.
- [17] H. Meng and Y. Li, "Fuzzy controller design for automatic carrier landing of aircraft," in *Proc. 33rd Chin. Control Conf.*, Nanjing, China, Jul. 2014, pp. 4457–4461.
- [18] K. Xia, S. Lee, and H. Son, "Adaptive control for multi-rotor UAVs autonomous ship landing with mission planning," *Aerosp. Sci. Technol.*, vol. 96, Jan. 2020, Art. no. 105549.
- [19] Y. Zhang, S.-H. Wang, B. Chang, and W.-H. Wu, "Adaptive constrained backstepping controller with prescribed performance methodology for carrier-based UAV," *Aerosp. Sci. Technol.*, vol. 92, pp. 55–65, Sep. 2019.
- [20] Z. Li and J. H. Park, "Dissipative fuzzy tracking control for nonlinear networked systems with quantization," *IEEE Trans. Syst., Man, Cybern. Syst.*, vol. 15, no. 2, pp. 509–519, Sep. 2018.
- [21] X.-H. Chang, J. Xiong, Z.-M. Li, and J. H. Park, "Quantized static output feedback control for discrete-time systems," *IEEE Trans. Ind. Informat.*, vol. 14, no. 8, pp. 3426–3435, Aug. 2018.
- [22] Q. Meng, T. Zhao, C. Qian, Z.-Y. Sun, and P. Ge, "Integrated stability control of AFS and DYC for electric vehicle based on non-smooth control," *Int. J. Syst. Sci.*, vol. 49, no. 7, pp. 1518–1528, Apr. 2018.
- [23] Q. Meng, C. Chen, P. Wang, Z. Sun, and B. Li, "Study on vehicle active suspension system control method based on homogeneous domination approach," *Asian J. Control*, vol. 2019, pp. 1–11, Sep. 2019.
- [24] N. Wada and S. Tsurushima, "Constrained MPC to track time-varying reference signals: Online optimization of virtual reference signals and controller states," *IEEE Trans. Electr. Electron. Eng.*, vol. 11, pp. S65–S74, Dec. 2016.
- [25] A. V. Rao, "A survey of numerical methods for optimal control," *Adv. Astron. Sci.*, vol. 135, no. 1, pp. 1–32, Jan. 2010.
- [26] D. Garg, M. Patterson, W. W. Hager, A. V. Rao, D. A. Benson, and G. T. Huntington, "A unified framework for the numerical solution of optimal control problems using pseudospectral methods," *Automatica*, vol. 46, no. 11, pp. 1843–1851, Nov. 2010.
- [27] X. Wang, H. Peng, S. Zhang, B. Chen, and W. Zhong, "A symplectic local pseudospectral method for solving nonlinear state-delayed optimal control problems with inequality constraints," *Int. J. Robust Nonlinear Control*, vol. 28, no. 6, pp. 2097–2120, Dec. 2017.
- [28] X. Wang, H. Peng, S. Zhang, B. Chen, and W. Zhong, "A symplectic pseudospectral method for nonlinear optimal control problems with inequality constraints," *ISA Trans.*, vol. 68, pp. 335–352, May 2017.
- [29] H. Peng, X. Wang, B. Shi, S. Zhang, and B. Chen, "Stabilizing constrained chaotic system using a symplectic pseudospectral method," *Commun. Nonlinear Sci. Numer. Simul.*, vol. 56, no. 2, pp. 77–92, Aug. 2017.
- [30] Y. Mao, D. Dueri, M. Szmuk, and B. Açikmeşe, "Successive convexification of non-convex optimal control problems with state constraints," *IFAC-PapersOnLine*, vol. 50, no. 1, pp. 4063–4069, Jul. 2017.
- [31] J. Liu, W. Han, X. Wang, and J. Li, "Research on cooperative trajectory planning and tracking problem for multiple carrier aircraft on the deck," *IEEE Syst. J.*, vol. 14, no. 2, pp. 3027–3038, Jun. 2020.
- [32] X. Wang, J. Liu, Y. Zhang, B. Shi, D. Jiang, and H. Peng, "A unified symplectic pseudospectral method for motion planning and tracking control of 3D underactuated overhead cranes," *Int. J. Robust Nonlinear Control*, vol. 29, no. 7, pp. 2236–2253, Feb. 2019.
- [33] M. B. Subrahmanyam, "H-infinity design of F/A-18A automatic carrier landing system," *J. Guid., Control, Dyn.*, vol. 17, no. 1, pp. 187–191, Jan. 1994.
- [34] Y. D. Yang, *Carrier Landing Guidance and Control*. Beijing, China: Defence Industry Press, 2006.
- [35] X. Wang, J. Liu, X. Su, H. Peng, X. Zhao, and C. Lu, "A review on carrier aircraft dispatch path planning and control on deck," *Chin. J. Aeronaut.*, Jul. 2020, doi: 10.1016/j.cja.2020.06.020.

- [36] H. Peng, "Symplectic Numerical Method for Computational Optimal Control and Its Application in the Control of Spacecraft near the Libration Point," Ph.D. dissertation, Dept. Eng. Mech., Dalian Univ. Technol., Dalian, China, 2012.
- [37] M. S. Bazaraa, H. D. Sherali, and C. M. Shetty, "Linear Complementarity Problem, and Quadratic, Separable, Fractional, and Geometric Programming," in *Nonlinear Programming: Theory Algorithms*. Hoboken, NJ, USA: Wiley, 2006, pp. 655–750.6.
- [38] J. Liu, W. Han, H. Peng, and X. Wang, "Trajectory planning and tracking control for towed carrier aircraft system," *Aerosp. Sci. Technol.*, vol. 84, pp. 830–838, Jan. 2019.
- [39] W. Kwon and A. Pearson, "A modified quadratic cost problem and feedback stabilization of a linear system," *IEEE Trans. Autom. Control*, vol. 22, no. 5, pp. 838–842, Oct. 1977.
- [40] Y. Meng, W. Wang, H. Han, and J. Ban, "A visual/inertial integrated landing guidance method for UAV landing on the ship," *Aerosp. Sci. Technol.*, vol. 85, pp. 474–480, Feb. 2019.
- [41] Y. Wang, "Stochastic analysis of nonstationary sequence," in *Applied Time Series Analysis*. Beijing, China: China Renmin Univ. Press, 2005, pp. 139–205.
- [42] M. D. Messina, "Simulation Model of the FA-18 High Angle-of-Attack Research Vehicle Utilized for the Design of Advanced Control Laws," Nat. Aeronaut. Space Admin. Langley Research Center, Hampton, Virginia, USA, NASA Technical Memorandum 110216, May 1996.
- [43] S. Ding and S. Li, "Second-order sliding mode controller design subject to mismatched term," *Automatica*, vol. 77, pp. 388–392, Mar. 2017.
- [44] Y. Yu, H. Wang, N. Li, Z. Su, and J. Wu, "Automatic carrier landing system based on active disturbance rejection control with a novel parameters optimizer," *Aerosp. Sci. Technol.*, vol. 69, pp. 149–160, Oct. 2017.



CONG SUN received the Ph.D. degree from Beihang University, China, in 2006. He is currently a Research Scientist with the Shenyang Aircraft Design and Research Institute, China. His research interests include the aircraft avionics and aircraft design.



XICHAO SU received the Ph.D. degree from Naval Aviation University, China, in 2018. He is currently a Lecturer with Naval Aviation University. His research interests include operation scheduling for aircraft and intelligent computation.



KAIKAI CUI received the M.S. degree from NUDT, China, in 2017. He is currently pursuing the Ph.D. degree with Naval Aviation University, China. His research interests include the general area of control and automation, and related fields such as aerodynamics.



WEI HAN received the Ph.D. degree from the Nanjing University of Aeronautics and Astronautics, China, in 2003. He is currently a Professor with Naval Aviation University, China. His research interests include the general area of the process industry control and automation, and related fields such as aerodynamics.



JIE LIU received the Ph.D. degree from Naval Aviation University, China, in 2019. He is currently an Assistant Researcher with the Academy of Military Sciences, China. His research interests include the control of unmanned ground systems, path planning for robots, and optimal control, and related fields, such as the process industry control and automation.

...